

## Electric Polarization of Soft Biological Tissues Induced by Ultrasound Waves

Kenji Ikushima<sup>1</sup>,\* Takashi Kumamoto, Kenshiro Ito, and Yamato Anzai

*Department of Biomedical Engineering, Tokyo University of Agriculture and Technology, Nakacho, Koganei, Tokyo 184-8588, Japan*



(Received 26 June 2019; published 3 December 2019)

Ultrasound irradiation makes it possible to generate alternating electric polarization through the electromechanical coupling of materials. It follows that electromagnetic fields are often emitted to the surrounding environment when materials are acoustically stimulated. We investigate the acoustically stimulated electromagnetic (ASEM) response of soft biological tissues. The ASEM signal is detected through a capacitive resonant antenna tuned to the MHz frequency of the irradiated ultrasound waves. The signal is well explained by the stress-induced polarization, which responds linearly to the applied acoustic stress. Induced polarization is clearly observed in the Achilles tendon, aortic wall, and aortic valve samples, whereas it is small in adipose tissue and myocardium samples, indicating that fibrous tissues exhibit electromechanical coupling.

DOI: 10.1103/PhysRevLett.123.238101

The strictest definitions of piezoelectricity only include single inorganic crystals that lack a center of symmetry [1]. When these materials are deformed, charges of opposite polarity appear on opposite faces of the crystal. However, the piezoelectric effect is also observed in inorganic polycrystalline or organic materials [2], and some biological tissues [3–7]. In polycrystalline materials, piezoelectricity results from the summation of electric dipole moments,  $\sum_i \mathbf{p}_i$ , produced by aggregations of partially oriented or quasicrystalline regions within the material.

Piezoelectricity in biological tissues was first discovered in dehydrated femoral cortex [3]. The microscopic unit of the crystalline structure of bone consists of inorganic hydroxyapatite (HAP) and collagen molecules. Because the unit cell of HAP belongs to a centrosymmetric space group ( $P6_3/m$ ), this inorganic component cannot exhibit piezoelectricity. In collagen, polypeptide chains form long rodlike molecules with short-range crystallinity [8]. The oriented collagen structure makes it responsible for piezoelectricity in bone.

However, the presence of piezoelectricity is still controversial in soft biological tissues. The piezoelectric properties of various types of dehydrated biological tissue, including the Achilles tendon, aortic wall, trachea, and intestines, have been reported [4–7]. In Ref. [5], the aortic wall sample was dehydrated under the tension for several weeks. The piezoelectric response was observed in the elongated aortic wall. The magnitude of the piezoelectric coefficient was estimated to be on the order of  $10^{-12}$  to  $10^{-15}$  C/N. In addition to macroscopic piezoelectric properties measured by tensile testing, piezoelectric properties at the nanometer scale have been studied using piezoresponse force microscopy [9–14]. Surprisingly, aortic walls and their main component, elastin, may also

be ferroelectric [13,14]. However, Lenz *et al.* found that both piezoelectric and ferroelectric properties are absent in aortic walls and did not observe a stress-induced charge [15]. Because the measurement techniques for piezoelectricity in soft biological tissues are limited to tensile testing or nanometer probe microscopy, an alternative method is required to verify the electromechanical properties. In addition, the electromechanical coupling in wet tissues will be more important biologically and medically [16]. However, it is usually difficult to evaluate the stress-induced charge on wet tissues owing to the formation of electric double layers. High-frequency measurements are required to avoid the effect of electric double layers or electrochemical transport [17]. Although piezoelectricity in wet bone has been investigated by applying MHz ultrasound modulation [18–21], the piezoelectric properties of wet soft tissues are still unknown.

In this Letter, we provide experimental evidence that fibrous soft biological tissues exhibit stress-induced polarization. The principle of our measurement technique is based on the generation and detection of the acoustically stimulated electromagnetic (ASEM) response through electro- or magnetomechanical coupling of materials [18]. In ferromagnetic materials, magnetization is modulated by ultrasound waves through magnetomechanical coupling. The first harmonic component of the acoustically induced magnetization has been detected using a resonant loop antenna tuned to the ultrasound frequency [22–24]. In this study, we focus on acoustically induced electric polarization that is detected by using a resonant capacitive antenna. The advantages of this technique are that (i) bulk and local electromechanical properties of soft tissues are obtained by spatial mapping with mesoscopic-scale resolution ( $\sim 1$  mm) and (ii) the stress-induced polarization in

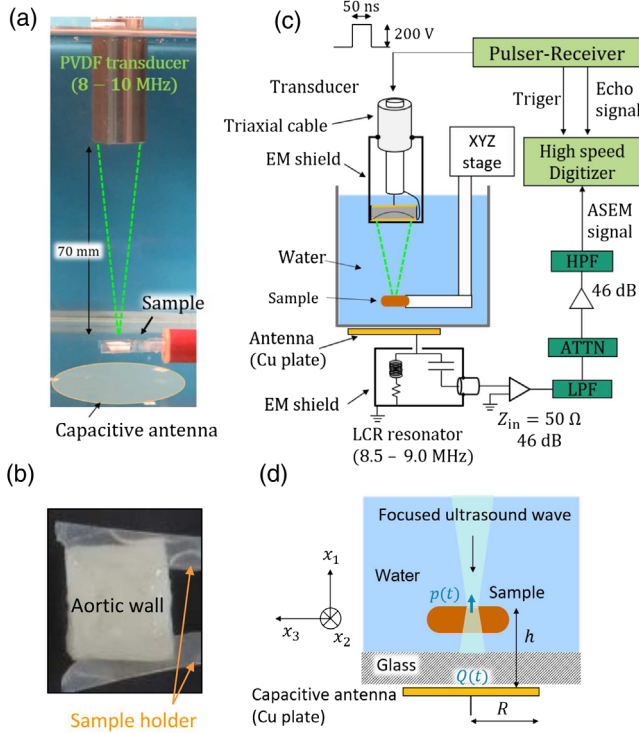


FIG. 1. (a) Photograph of the experimental setup. (b) Photograph of an aortic wall sample set in a plastic sample holder. (c) Block diagram of the ASEM measurement system. (d) Schematics of the geometric placement in the sample setting.

wet soft tissues is measured by high-frequency ultrasound modulation.

Porcine aortic wall (size:  $9 \times 10 \times 2$  mm), aortic valve (size:  $10 \times 20 \times 4$  mm), myocardium (size:  $7 \times 5 \times 2$  mm), and abdominal adipose tissue (size:  $10 \times 10 \times 7$  mm) samples are prepared as described in Sec. A of the Supplemental Material [25]. Bovine Achilles tendon samples (size:  $12 \times 10 \times 6$  mm<sup>3</sup>) are used. These tissues are kept at  $-20^\circ\text{C}$  and are thawed and rinsed in deionized water for about 30 min before performing measurements. The thawed tissues are set in a plastic sample holder and submerged in a glass tank of deionized water [Figs. 1(a) and 1(b)].

The block diagram of the experimental setup is shown in Fig. 1(c). Rectangular 50-ns-wide pulses are applied to a broadband polyvinylidene fluoride (PVDF) transducer (peak frequency: 8–10 MHz) using a pulser-receiver (5077PR, Panametrics-NDT). An appropriate distance between the sample and transducer (70 mm in this experiment) allows us to separate the pulsed ASEM response from the EM noise generated by the transducer temporally [18]. The ASEM signal is detected by a resonant capacitive antenna tuned to the frequency of the ultrasound waves. The antenna is a copper plate coupled with a *LCR* resonator [Lorentzian-shape spectrum,  $L(\omega - \omega_0, \Gamma)$ ; central frequency,  $\omega_0 = 8.67$  MHz; bandwidth,  $2\Gamma = 810$  kHz]. Signals picked up by the antenna are amplified by 92 dB and typically averaged over  $3 \times 10^4$  pulses at a repetition

frequency of 1 kHz. The focal spot is set to be on the surface of the samples (radius of the focal spot:  $\Delta r = 0.65$  mm). The amplitude of the acoustic stress  $T_{ac}$  is measured by using a calibrated broadband PVDF hydrophone. The frequency spectrum of the pulsed ultrasound wave  $f(\omega)$  is much broader than the *LCR* resonator detection spectrum,  $L(\omega - \omega_0, \Gamma)$ . The amplitude of acoustic stress  $T_{ac}(\omega_0)$  at the resonance frequency is numerically calculated as the Fourier component  $T_{ac}(\omega_0) = \int f(\omega)L(\omega - \omega_0, \Gamma)d\omega$  for a given excitation pulse voltage  $V_{pulse}$ .  $T_{ac}$  versus  $V_{pulse}$  is linear up to 200 V, and the conversion coefficient from excitation pulse voltage to acoustic stress is 12.7 Pa/V. All major measurements are performed by applying a 200 V excitation pulse corresponding to  $T_{ac} = 3.2$  kPa. Spatial images are obtained by moving the sample using an *XYZ* stage. The spatial resolution  $\Delta x$  of the ASEM response is determined by the time constant in the detection system that corresponds to the bandwidth of the *LCR* resonator. The lateral spread of the focal spot due to propagation is estimated to be  $\Delta x = v\Delta t \sim 1.8$  mm, using  $v = 1500$  m/s and  $\Delta t = 1/(2\Gamma) \simeq 1.2$   $\mu\text{s}$ . Thus, the acoustically excited area is roughly estimated to be  $S_{ex} = \pi(\Delta r + \Delta x)^2 = 1.9 \times 10^{-5}$  m<sup>2</sup> [25]. Ultrasound waves are irradiated perpendicular to the fiber orientation of the fibrous tissues [Fig. 1(d)] [28].

Figures 2(a) and 2(b) show the time traces of the echo and ASEM signals for the Achilles tendon sample. The distance  $h$  between the focal spot and the metal antenna is set as 21 mm for an antenna radius  $R$ , of 15 mm ( $h/R = 1.4$ ). Because the ASEM response is generated at half the echo delay time  $\tau_{echo}/2$ , the signal observed at 47  $\mu\text{s}$  is identified as the target ASEM response of the Achilles tendon sample [Fig. 2(b)]. The signal from the water tank glass plate is also observed around 57  $\mu\text{s}$  when the sample is sufficiently transparent to ultrasound waves. The secondary signal around 70  $\mu\text{s}$  is attributed to the ASEM response from the tissue induced by ultrasound waves reflected from the glass plate. A similar ASEM response is observed for the aortic wall [Fig. 2(c)] and aortic valve [Fig. 2(d)] samples, whereas the ASEM response is small in the adipose tissue [Fig. 3(a)] and myocardium [Fig. 3(b)] samples. These results indicate that fibrous soft tissues exhibit relatively large electromechanical coupling.

Figures 4 and 5 show spatial images of the echo and ASEM signals for the Achilles tendon and aortic wall samples, respectively. The spatial distribution of ASEM signals does not necessarily correspond to that of the echo signals. Because biological tissues are complex inhomogeneous materials, the signal amplitudes depend on the measurement positions with a variance of about 50%. The spatially averaged ASEM signal amplitude and its variance are estimated to be  $\langle V_{sig} \rangle \pm \delta V_{sig} = 82 \pm 36$  and  $113 \pm 55$  nV for the Achilles tendon and aortic wall samples, respectively. In the tomographic images [Fig. 4(d)], the ASEM signal is generated mainly on the

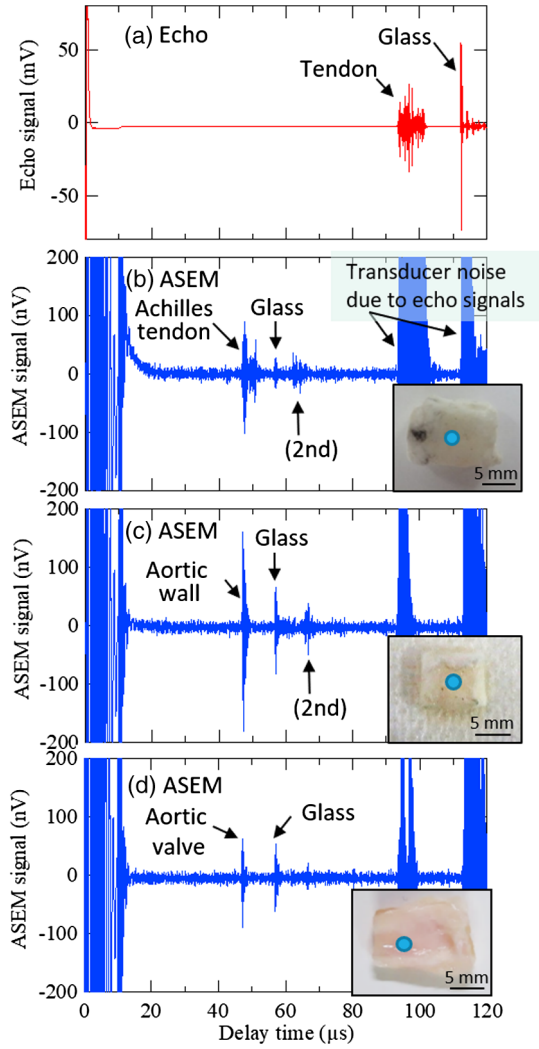


FIG. 2. Typical time traces of (a) echo signals in the Achilles tendon and time traces of ASEM signals in (b) the Achilles tendon, (c) aortic wall (intima side), and (d) aortic valve. The data are taken for  $h = 21$  mm ( $h/R = 1.4$ ). The insets show photographs of the samples. The circles in the insets indicate the positions of the measurements.

surface of the tendon tissue. On the other hand, the aortic wall consists of the intima, media, and adventitia layers [29]. Figure 5 shows the imaging results for the aortic wall sample obtained by irradiating the ultrasound waves from the adventitia side. Because of the lack of time resolution (corresponding to depth resolution  $\Delta x$ ), the individual layers of the aortic wall are not clearly identified in the ASEM tomography [Fig. 5(d)]. The signal amplitude was almost the same as that measured by ultrasound irradiation from the intima side.

We show that the ASEM response originates from the acoustically induced electric polarization in soft biological tissues. In polycrystalline substances, locally induced polarization can be expressed as  $P_{\text{loc}} = \bar{p}(t)/V \simeq q_{\text{dip}}(t)l/V$ , where  $\bar{p}(t)$  is the summation of electric dipole moment  $|\sum_i \mathbf{p}_i|$  induced in the excited area  $S_{\text{ex}}$ ,  $V$  is the excited

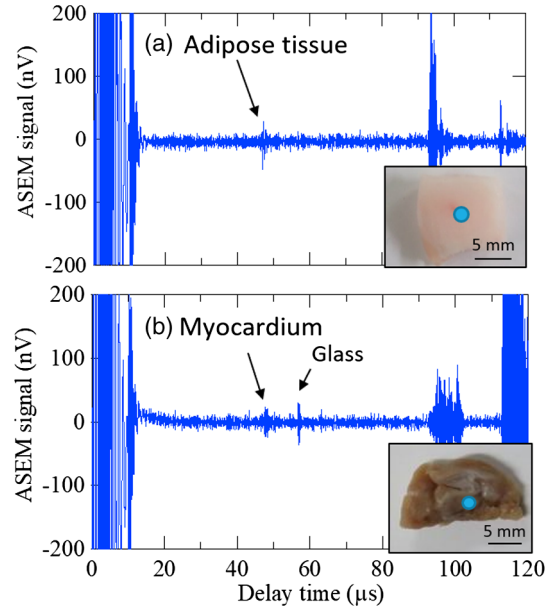


FIG. 3. Typical time traces of ASEM signals of (a) adipose tissue (porcine) and (b) myocardium (porcine). The data are taken for  $h = 21$  mm ( $h/R = 1.4$ ). The insets show photographs of the samples. The circles in the insets indicate the positions of the measurements. We checked the spatial distribution of the ASEM response by two-dimensional mapping (more than 200 positions) for individual tissues. The spatially averaged ASEM signal amplitude of both tissues is estimated to be about 20 nV, which corresponds to the detection limit in our measurement setup.

volume,  $S_{\text{ex}}l$ , and  $l$  is the displacement between opposite effective charges,  $\pm q_{\text{dip}}(t)$ . The of  $l$  is on the order of half the wavelength of the ultrasound waves ( $l = \lambda/2 \sim 0.1$  mm). When an alternating electric dipole moment along the

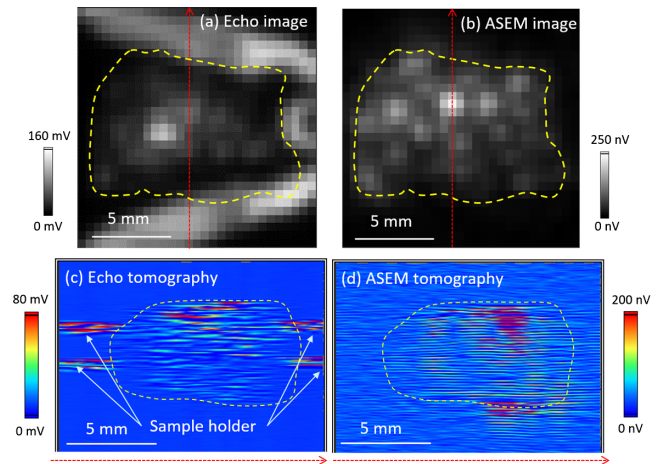


FIG. 4. Imaging of the Achilles tendon sample. (a) Echo lateral image, (b) ASEM lateral image, (c) echo tomographic image (B mode), and (d) ASEM tomographic image. The dotted red arrows in (a) and (b) indicate the position of the tomographic images shown in (c) and (d), respectively. The dashed yellow curves show the surface form of the sample. The data are taken for  $h = 21$  mm ( $h/R = 1.4$ ).

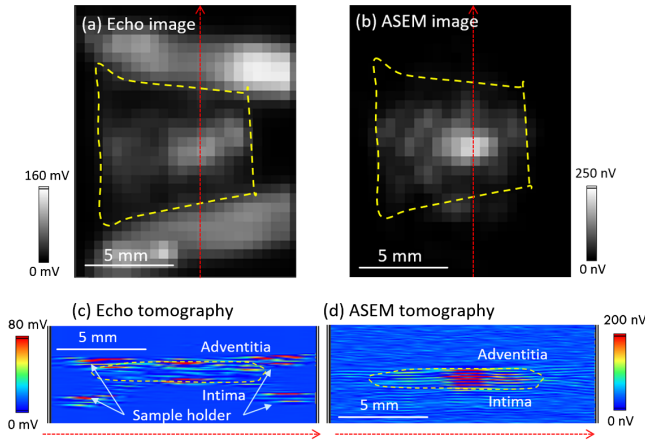


FIG. 5. Imaging of the aortic wall sample. (a) Echo lateral image, (b) ASEM lateral image, (c) echo tomography (B mode), and (d) ASEM tomography. Ultrasound waves are irradiated from the adventitia side of the aortic wall. The dotted red arrows in (a) and (b) indicate the position of the tomographic images shown in (c) and (d), respectively. The dashed yellow curves show the surface form of the sample. The data are taken for  $h = 21$  mm ( $h/R = 1.4$ ).

$x_1$  axis,  $\bar{p}(t) = q_{\text{dip}} l \sin \omega_0 t$ , is locally generated with an ultrasound frequency of  $\omega_0$ , a surface charge  $Q(t) = Q_0 \sin \omega_0 t$  is induced on the planar metal antenna [Fig. 6(a)]. In this dipole detection model,  $Q_0$  multiplied by  $R$  is expressed as a function of a single variable  $h/R$  by [25]

$$Q_0 \times R = q_{\text{dip}} l [1 + (h/R)^2]^{-3/2}. \quad (1)$$

The amplitude of the signal voltage  $V_{\text{sig}}$  multiplied by  $R$  is also expressed as

$$V_{\text{sig}} \times R = V_0 R [1 + (h/R)^2]^{-3/2}, \quad (2)$$

where  $V_0$  corresponds to the signal amplitude for  $h/R \rightarrow 0$  and  $V_0 R$  is independent of the antenna radius  $R$ . The polarization charge  $q_{\text{dip}}$  is obtained by

$$q_{\text{dip}} = \frac{2V_0 R}{Z_{\text{in}} \omega_0 l} \simeq \frac{2V_0 R}{\pi v_{\text{ac}} Z_{\text{in}}}, \quad (3)$$

where  $Z_{\text{in}}$  is the input impedance of the preamplifier  $Z_{\text{in}} = 50 \Omega$  and  $v_{\text{ac}}$  is the acoustic velocity of longitudinal waves in the biological tissues (1700 m/s for tendon [30] and 1590 m/s for aortic wall [31]). The  $h/R$  dependences of  $V_{\text{sig}} \times R$  for the Achilles tendon and aorta wall are shown in Fig. 6(b), where the signals are measured by using two antennas with  $R = 15$  and 30 mm. The signal voltage  $V_{\text{sig}}$  is well scaled by multiplying the antenna radius  $R$ , which strongly supports the model of acoustically induced electric polarization. The experimental data are fitted to Eq. (2), and the values of  $V_0 R$  are evaluated as 7.66 and 11.3 nV m for the Achilles tendon and aortic wall, respectively. Accordingly,

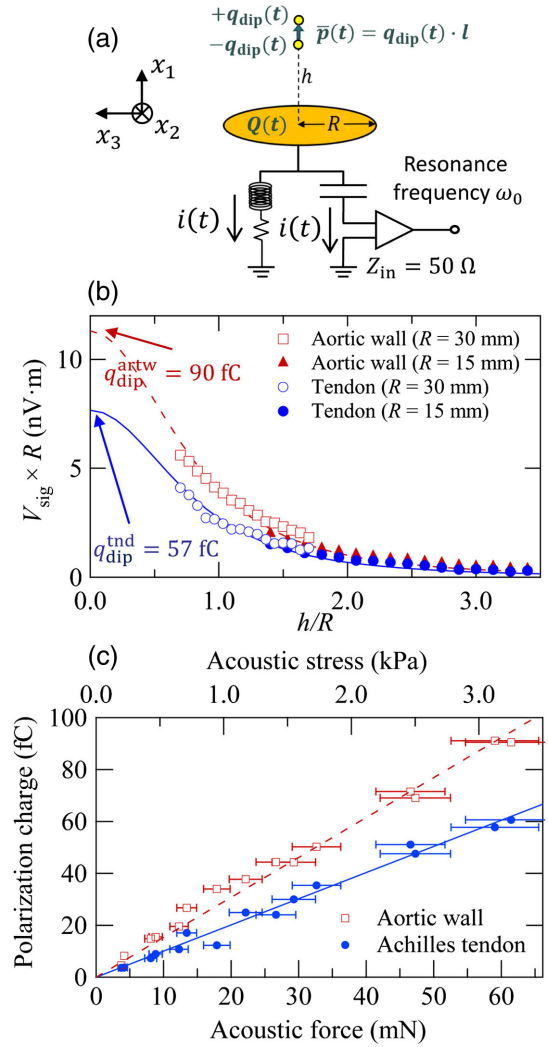


FIG. 6. (a) Schematic of the dipole detection model. (b) Signal amplitude multiplied by  $R$  as a function of  $h/R$  for the Achilles tendon and aortic wall samples. The solid and dashed lines represent the best-fit curves based on the dipole detection model for the Achilles tendon and aortic wall, respectively. (c) Induced polarization charge  $q_0$  as a function of acoustic force  $F_{\text{ac}}$  for the Achilles tendon and aortic wall samples. The data are taken for  $h = 21$  mm ( $h/R = 1.4$ ).

the induced polarization charges for the Achilles tendon and aortic wall are estimated to be  $q_{\text{dip}}^{\text{tnd}} = 57$  and  $q_{\text{dip}}^{\text{artw}} = 90$  fC, respectively.

We also investigate the stress dependence of the polarization charge. The piezoelectric response is generally written as a function of frequency  $P_{\text{loc}}(\omega_0) = d_{\text{loc}}(\omega_0) T_{\text{ac}}(\omega_0)$ , where  $d_{\text{loc}}$  is the local piezoelectric coefficient in the acoustically excited area. Using the acoustic force  $F_{\text{ac}} = T_{\text{ac}} S_{\text{ex}}$  the piezoelectric response can be rewritten as  $q_{\text{dip}}(\omega_0) = d_{\text{loc}}(\omega_0) F_{\text{ac}}(\omega_0)$ . As shown in Fig. 6(c), the polarization charge  $q_{\text{dip}}$  exhibits linear behavior in the measurement range. Thus,  $d_{\text{loc}}$  is roughly estimated to be  $\sim 1$  pC/N for the Achilles tendon and  $\sim 2$  pC/N for the aortic

wall. These values are comparable to the static piezoelectric coefficient ( $\sim 1$  pC/N) reported for the dehydrated tendon or aortic wall [4,5,13].

We investigated the stress-induced polarization in soft biological tissues by detecting the first harmonic component of the acoustically induced electric fields. Polarization was observed in Achilles tendon, aortic wall, and aortic valve samples, whereas it was small in adipose tissues and myocardium samples, indicating that fibrous soft tissues exhibit electromechanical coupling even in wet conditions. The polarization responded linearly to acoustic stress in the measurement range. A naive question on the ferroelectricity of aortic walls still remains, but our study settles an argument on the presence of stress-induced polarization in the aortic wall. We also demonstrated lateral and tomographic imaging of stress-induced polarization in soft biological tissues. This noninvasive imaging technique could help to explore electromechanical coupling of various soft materials, even in living tissues.

We are grateful to H. Yamada, N. Ohno, S. Naito, K. Watanabe, and K. Fukumoto from Tokyo University of Agriculture and Technology for collaboration in the early stages of this work. We would like to thank Y. Yabe and Y. Hagiwara from the Department of Orthopaedic Surgery, Tohoku University, and N. Niimi and Y. Kojima from Nippon Sigmax Co., Ltd. for simulating discussions on fibrous biological tissues. This work is financially supported by JSPS KAKENHI Grants No. JP17H02808 and No. JP19K22956.

\*ikushima@cc.tuat.ac.jp

- [1] W. G. Cady, *Piezoelectricity* (Mc Graw-Hill Co., New York, 1946), p. 806.
- [2] J. Duchesne, J. Depireus, A. Bertinchamps, N. Comet, and J. M. Van der Kaa, *Nature (London)* **188**, 405 (1960).
- [3] E. Fukada and I. Yasuda, *J. Phys. Soc. Jpn.* **12**, 1158 (1957).
- [4] E. Fukada and I. Yasuda, *Jpn. J. Appl. Phys.* **3**, 117 (1964).
- [5] E. Fukada and K. Hara, *J. Phys. Soc. Jpn.* **26**, 777 (1969).
- [6] E. Fukada, *Biorheology* **32**, 593 (1995).
- [7] E. Fukada, *Adv. Biophys.* **6**, 121 (1974).
- [8] M. D. Shoulders and R. T. Raines, *Annu. Rev. Biochem.* **78**, 929 (2009).
- [9] S. V. Kalinin, A. Rar, and S. Jesse, *IEEE Trans. Ultrason. Ferroelectr. Freq. Control* **53**, 2226 (2006).
- [10] A. Gruverman and S. V. Kalinin, *J. Mater. Sci.* **41**, 107 (2006).
- [11] S. V. Kalinin, B. J. Rodriguez, S. Jesse, E. Karapetian, B. Mirman, E. A. Eliseev, and A. N. Morozovska, *Annu. Rev. Mater. Res.* **37**, 189 (2007).
- [12] D. A. Bonnel, S. V. Kalinin, A. L. Kholkin, and A. Gruverman, *MRS Bull.* **34**, 648 (2009).
- [13] Y. Liu, Y. Zhang, M.-J. Chow, Q. N. Chen, and J. Li, *Phys. Rev. Lett.* **108**, 078103 (2012).
- [14] Y. Liu, H.-L. Cai, M. Zelisko, Y. Wang, J. Sun, F. Yan, F. Ma, P. Wang, Q. N. Chen, H. Zheng, X. Meng, P. Sharma, Y. Zhang, and J. Li, *Proc. Natl. Acad. Sci. U.S.A.* **111**, E2780 (2014).
- [15] T. Lenz, R. Hummel, I. Kastouras, W. A. Groen, M. Nijemeisland, R. Ruemmler, M. K. E. Schäfer, and D. M. de Leeuw, *Appl. Phys. Lett.* **111**, 133701 (2017).
- [16] C. A. L. Bassett, *Calcified Tissue Research* **1**, 252 (1967).
- [17] A. C. Ahn and A. J. Grodzinsky, *Medical Engineering and Physics* **31**, 733 (2009).
- [18] K. Ikushima, S. Watanuki, and S. Komiyama, *Appl. Phys. Lett.* **89**, 194103 (2006).
- [19] M. Okino, S. Coutelou, K. Mizuno, T. Yanagitani, and M. Matsukawa, *Appl. Phys. Lett.* **103**, 103701 (2013).
- [20] H. Tuneda, S. Matsukawa, S. Takayanagi, K. Mizuno, T. Yanagitani, and M. Matsukawa, *Appl. Phys. Lett.* **106**, 073704 (2015).
- [21] S. Matsukawa, T. Makino, S. Mori, D. Koyama, S. Takayanagi, K. Mizuno, T. Yanagitani, and M. Matsukawa, *Appl. Phys. Lett.* **110**, 143701 (2017).
- [22] H. Yamada, K. Takashima, K. Ikushima, H. Toida, M. Sato, and Y. Ishizawa, *Rev. Sci. Instrum.* **84**, 044903 (2013).
- [23] H. Yamada, K. Watanabe, and K. Ikushima, *Jpn. J. Appl. Phys.* **54**, 086601 (2015).
- [24] H. Yamada, J. Yotsuji, and K. Ikushima, *Jpn. J. Appl. Phys.* **57**, 07LB09 (2018).
- [25] See Supplemental Material at <http://link.aps.org/supplemental/10.1103/PhysRevLett.123.238101> for sample preparation (Sec. A) and the detail information of the charge and dipole detection models, which includes Refs. [18,26,27].
- [26] D. A. Berlincourt, D. R. Curran, and H. Jaffe, *Physical Acoustics* (Academic Press, New York and London, 1964), Vol. 1-Part A, pp. 169–270.
- [27] E. Fukada, *IEEE Trans. Ultrason. Ferroelectr. Freq. Control* **47**, 1277 (2000).
- [28] A summation of piezoelectric polarization  $\mathbf{P}_1 = \sum_{i=1}^6 d_i T_i$  will be detected by the capacitive antenna. See Sec. B in the Supplemental Material [25].
- [29] J. A. G. Rhodin, *Architecture of the Vessel Wall* (American Physiological Society, 2011), pp. 1–31.
- [30] C. A. Miles, *J. Acoust. Soc. Am.* **99**, 3225 (1996).
- [31] D. J. Hughes and B. Snyder, *Med. Biol. Eng. Comput.* **18**, 220 (1980).